Hindawi
International Journal of Aerospace Engineering
Volume 2018, Article ID 1678709, 16 pages
https://doi.org/10.1155/2018/1678709

Research Article

Design Methodology and Performance Evaluation of New Generation Sounding Rockets

Marco Pallone, Mauro Pontani, Paolo Teofilatto, and Angelo Minotti

University of Rome "La Sapienza", Via Salaria 851/831, 00138 Rome, Italy

Correspondence should be addressed to Marco Pallone; pallone.1420138@studenti.uniroma1.it

Received 24 March 2017; Accepted 25 September 2017; Published 6 February 2018

Academic Editor: Corin Segal

Sounding rockets are currently deployed for the purpose of providing experimental data of the upper atmosphere, as well as for microgravity experiments. This work provides a methodology in order to design, model, and evaluate the performance of new sounding rockets. A general configuration composed of a rocket with four canards and four tail wings is sized and optimized, assuming different payload masses and microgravity durations. The aerodynamic forces are modeled with high fidelity using the interpolation of available data. Three different guidance algorithms are used for the trajectory integration: constant attitude, near radial, and sun-pointing. The sun-pointing guidance is used to obtain the best microgravity performance while maintaining a specified attitude with respect to the sun, allowing for experiments which are temperature sensitive. Near radial guidance has instead the main purpose of reaching high altitudes, thus maximizing the microgravity duration. The results prove that the methodology at hand is straightforward to implement and capable of providing satisfactory performance in term of microgravity duration.

1. Introduction

Sounding rockets are specialized missiles generally used to investigate the region of space between 50 and 700 km where it is difficult to enter with the traditional atmospheric balloon or low orbit satellites. They can be used in several missions, such as detection of the solar activity and anomalies, analysis of the constituents of the upper atmosphere, thermal analysis on new materials, and generally, measurements of the space surrounding the Earth [1–3]. The most important characteristic of a sounding rocket is the capability of achieving microgravity conditions for the payload, without the need of a manned mission in the ISS to perform experiments and then reducing the costs of the mission. The quality of microgravity depends on the absence of drag and other gyroscopic forces, so the guidance of the rocket assumes the utmost importance. Another good characteristic of the sounding rocket in contrast to the satellite missions is the sounding rocket's ability to retrieve the payload with the help of a heat shield and a parachute. For all of these reasons, a vast number of sounding rocket families were developed, such as the American "Black Brant" and the European "Maxus." The Black Brant family includes sounding rockets that range from one through three stages. The Black Brant VC [4] (Figure 1) can be launched from a steerable launch tower with different kick angles to achieve different apogee altitudes. It is controlled via spin-up motors and canard wings, which provide a fast response at the cost of small instability. Four rear tail surfaces guarantee an adequate static margin. The Maxus [4, 5] is a very powerful European single-stage sounding rocket launched in Kiruna (Sweden) and can reach a maximum altitude of 700 km, while the range does not exceed 100 km. It has a microgravity duration of about 12 min, and the microgravity level Δg is near 10^{-4}m/sec^2. TVC control system is highly sophisticated in order to guarantee strict margins for the range and to avoid damages to both people and goods. Table 1 portrays some useful data to compare the performance of the two rockets.

Both of these sounding rockets are propelled with a solid state motor, due to their simplicity and light weights with respect to liquid propellant. A crucial point is that a sounding rocket has to be cheaper than a high-tech rocket, and in order to achieve this objective, new design methodologies are needed. Many authors (e.g., Chowdhury et al. [6, 7] and

Figure 1: Black Brant VC.

Table 1: "Maxus" and "Black Brant VC" data.

	BBVC	Maxus
Length (m)	8.3	16.2
Max diameter (m)	0.44	1
Mass liftoff (kg)	1544	12298
Propellant mass (kg)	1017	10042
Av. thrust (N)	69374	372500
Burnout time (sec)	32	63

Casalino and Pastrone [8, 9]) are interested in designing new sounding rockets to explore the potentiality of new hybrid motors for hypersonic flight. Nonaka et al. [10] and Woo et al. [11] investigated the reusability of the sounding rocket, and Cremaschi et al. [12] investigated the optimization of a trajectory with the use of a commercial trajectory simulation tool (ASTOS). However, a very limited number of studies are concerned with fast sizing and aerodynamic losses during the ascent path. The purpose of this work is to find a novel and simple methodology to size and design for future sounding rockets, considering accurate aerodynamics and three guidance algorithms. In particular, the technique explained in this work is applied to a single-stage rocket whose three-dimensional trajectory is simulated using the following guidance schemes:

(i) Constant attitude guidance

(ii) Near radial guidance

(iii) Sun-pointing guidance

This work purpose is to find a procedure that can provide the minimal volume rocket that can guarantee a fixed time of microgravity with different scientific payloads inside. Definitely, the methodology at hand yields configurations that can provide a well-developed preliminary design for future sounding rockets, with an accurate aerodynamic model and using three distinct guidance schemes.

2. Rocket Geometry and Sizing

2.1. Basic Geometry. With the purpose of maintaining the configuration as simple as possible, the sounding rocket is composed of one stage and a module hosting the avionics, experiments, and recovery system (parachute and the heat shield).

The basic geometry of the rocket is composed of the following:

(i) A nose cone of parabolic shape

(ii) A fuselage of cylindrical shape

(iii) Four canard wings in cruciform configuration

(iv) Four tail surfaces of trapezoidal shape

This configuration is chosen with the purpose of creating an algorithm as general as possible. Incidentally, this geometry is adopted by a lot of sounding rockets in the market, like the "Black Brant VC" in Figure 1.

Every rocket configuration in this work is defined by the total length l and the maximum diameter d, while all the other parameters like the propulsive ones are obtained through scaling factors. The grid used for the computation is

(i) l from 3 m to 15 m with step of 1 m

(ii) d from 0.2 m to 1.5 m with step of 0.05 m.

Thus, a total of 243 different configurations were analyzed. The design methodology that is being presented relates geometry, weight, aerodynamics, and propulsive performances.

2.2. Main Body. For each configuration, the length of the ogive is proportional to the total length of the sounding rocket

$$l_{\text{ogive}} = C_{\text{ogive}} l, \tag{1}$$

where $C_{\text{ogive}} = 0.17$ is a dimensionless coefficient. The dimensional ogive point distribution is then obtained by multiplying the nondimensional points in the (ξ, η) frame in Figure 2 with l_{ogive} and d. The main body, which contains the propulsive system and the avionics, is cylindrical with diameter d, while its length is found through

$$l_{\text{body}} = l - l_{\text{ogive}}. \tag{2}$$

2.3. Aerodynamic Surfaces. The aerodynamic surfaces are sized according to the following ratios:

$$\begin{aligned} A_{\text{P}} &= \left(l - l_{\text{ogive}}\right) d, \\ A_{\text{C}} &= \frac{1}{45} A_{\text{P}}, \\ A_{\text{T}} &= \frac{1}{12} A_{\text{P}}. \end{aligned} \tag{3}$$

Then the following quantities are computed as follows:

$$\begin{aligned} h_{\text{T}} &= \sqrt{\frac{4}{3} A_{\text{C}}}, \\ h_{\text{C}} &= \sqrt{2 A_{\text{T}}}, \end{aligned} \tag{4}$$

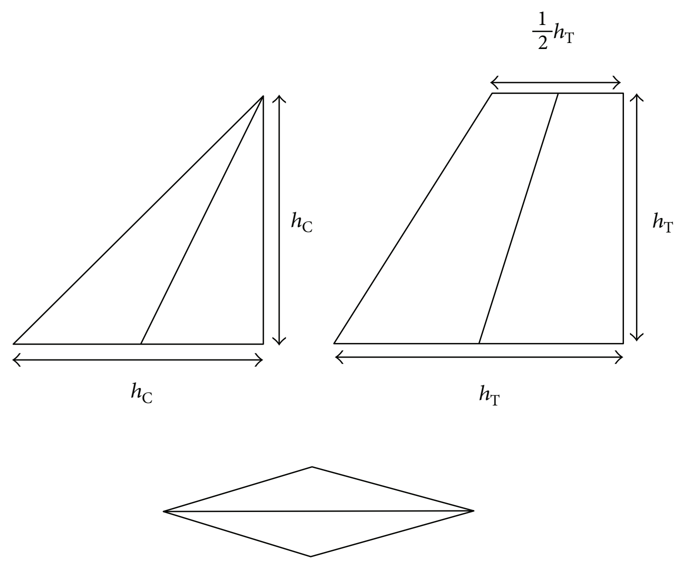

(a) Canard and tail wing geometry. The profile adopted is a symmetric double-wedge profile

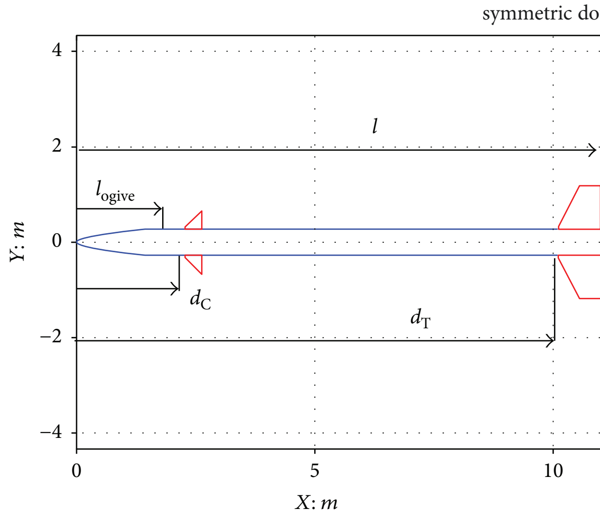

(b) Canard and tail wing disposition along the longitudinal axis

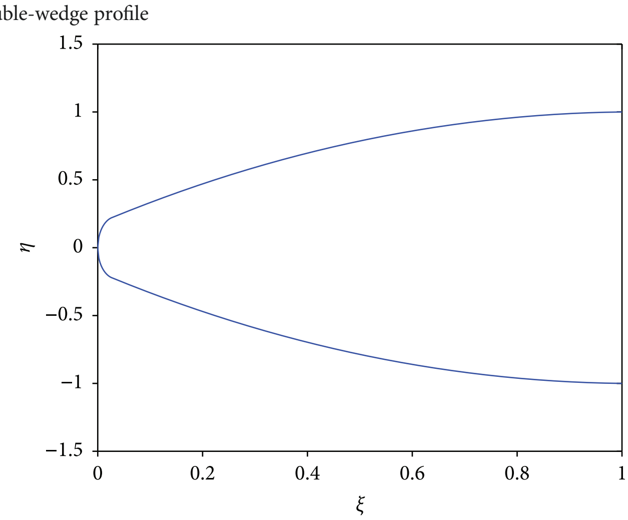

(c) Nondimensional ogive

Figure 2: Main surfaces and reference quantities.

while the distances with respect to the nose tip are as follows:

$$d_C = l_{ogive} + 0.4\text{m},$$
$$d_T = l - h_T. \tag{5}$$

The main concept under this procedure is to maintain the shape of the wings, while selecting their size in relation to the overall size of the main body. This is in order to avoid wings with nonconventional shapes that would result in undesired aerodynamic effects. Figure 2 portrays the wing geometry with the profile adopted for both wing systems. The nonvariable distance in (5) 0.4 m is meant to provide a fixed volume needed for the canard avionic and the recovery system. Figure 2 portrays an example of a configuration with the disposition of the leading edges along the longitudinal axis of the rocket.

Table 2: Auxiliary mass m_{aux} of the ogive.

Parachute mass (kg)	10
Heat shield mass (kg)	35
Metal case mass (kg)	5
Total m_{aux} (kg)	50

2.4. Mass Scaling. In order to describe properly a real sounding rocket mission, a fixed mass including parachute, heat shield, and metal case is used for every configuration. Table 2 portrays in detail these auxiliary masses, which form m_{aux}.

With regard to the initial mass at launch, a common initial density is used in order to find a reasonable and scaled mass distribution for every rocket configuration. This initial density is $C_{m_0} = 1092.3\text{kg/m}^3$, which is taken from the Black

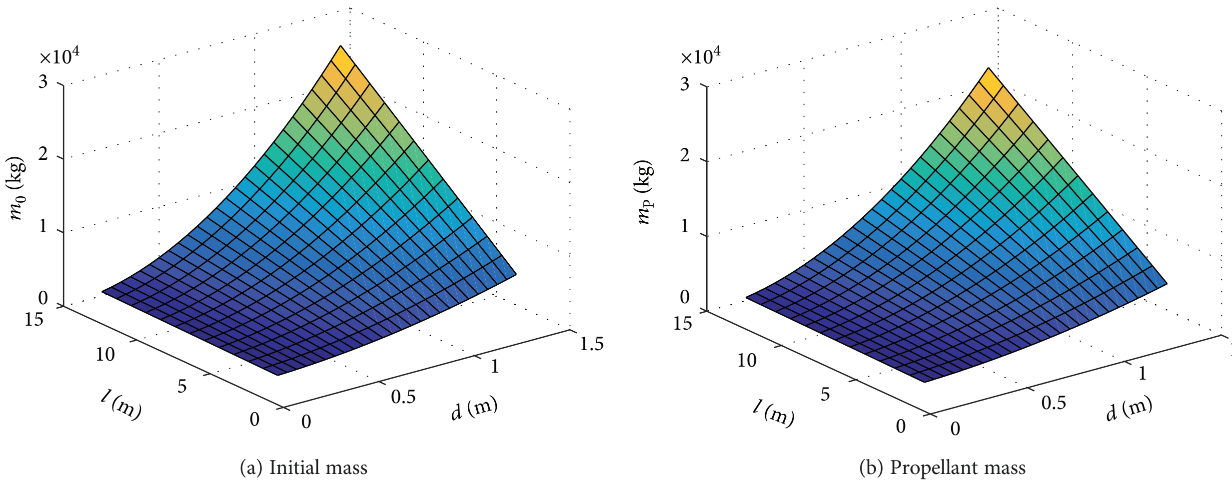

FIGURE 3: Example of scaled m_0 and m_P with $m_U = 50$kg.

Brant VC and is considered to have a reasonable value. This value includes propellant, structural, and auxiliary masses. So the initial mass for every configuration without the ogive mass is

$$m_{0\text{body}} = C_{m_0} V_{\text{body}}. \tag{6}$$

For every configuration. 50, 100, and 200 kg of scientific payload are used, so the total initial mass at launch is

$$m_0 = m_{0\text{body}} + m_U + m_{\text{aux}}. \tag{7}$$

The propulsive technology of this single-stage rocket is a solid propellant one, allowing for the following structural coefficient:

$$\epsilon = \frac{m_S}{m_P + m_S} = 0.11. \tag{8}$$

The structural and propellant masses are obtained through the following expressions:

$$\begin{aligned} u &= \frac{m_U + \epsilon m_0 - \epsilon m_U}{m_0}, \\ m_P &= \frac{m_0}{1-u}, \\ m_S &= \frac{\epsilon m_0 (1-u)}{1-\epsilon}. \end{aligned} \tag{9}$$

In the end, (6), (7), (8), and (9) yield the overall rocket mass at launch, portrayed in Figure 3 as a function of l and d, together with the corresponding propellant mass.

2.5. Propulsion System Scaling. To scale the thrust for every sounding rocket size, the initial launch acceleration and the specific impulse are maintained constant:

$$T = n_0 g m_0, \tag{10}$$

where $n_0 = 3g$, while the propellant mass consumption is

$$\dot{m} = -\frac{T}{I_{sp} g}. \tag{11}$$

The value for n_0 is chosen in order to constrain the rocket dynamical stress at launch. Equation (11) leads to the burnout time:

$$t_B = \frac{m_P}{\dot{m}}. \tag{12}$$

Figure 4 portrays the thrust and the burnout time scaling with the rocket size.

3. Rocket Aerodynamic Modeling

Aerodynamic forces affect the rocket motion, which partially occurs in the atmosphere. Thus, the rocket aerodynamics is to be modeled appropriately. In this work, four quantities are assumed to determine the aerodynamic forces: Mach number M, Reynolds number Re, angle of attack α, and sideslip angle β. To provide an accurate model for each configuration, two fundamental steps are needed:

(1) Derivation of the aerodynamic coefficients C_D, C_L, and C_Q from DATCOM [13] at a relevant number of Mach, Reynolds, angles of attack, and sideslip angles

(2) Cubic interpolation of the aerodynamic coefficients during the integration of the dynamics equations

Following the approach presented by Mangiacasale [14], Pallone et al. [15], and Pontani [16], the aerodynamics of the rocket was modeled through the Missile DATCOM software [13]. This software provides an accurate esteem of the aerodynamic forces without using a lot of computational resources; thus, it can provide a complete aerodynamic database for each configuration in a short time. The following discrete values of M, Re, α, and β are used:

(i) $M = [0.2, 0.5, 0.6, 0.8, 0.9, 1.1, 1.2, 1.5, 2, 2.5, 3, 3.5, 4, 4.5, 5, 5.5, 6, 6.5, 7, 7.5, 8, 10]$

(ii) $\text{Re} = [0.5, 1, 1.5, 2] * 10^5$

(iii) $\alpha = [0, 1, 2, 3, 4, 5]$ deg

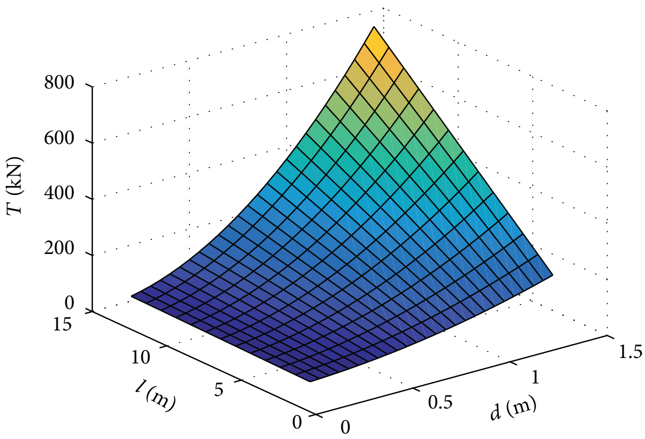

(a) Thrust

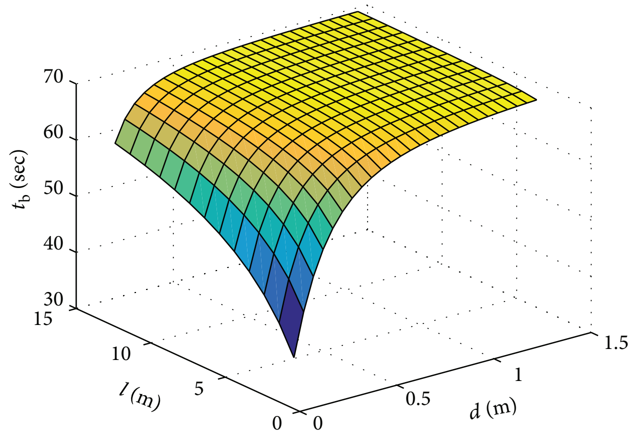

(b) Burnout time

FIGURE 4: Example of scaled T and t_B with $m_U = 50$ kg.

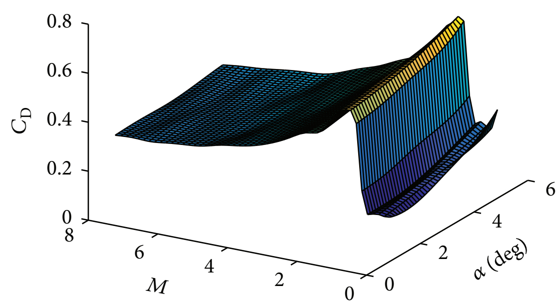

(a) Drag coefficient for $\beta = 0$ deg and $\mathrm{Re} = 4 * 10^7$

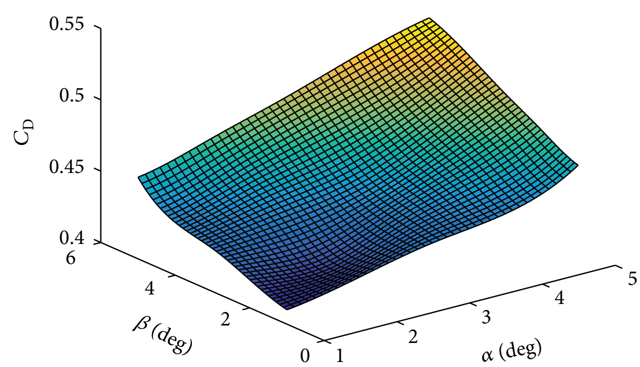

(b) Drag coefficient for $M = 3$ and $\mathrm{Re} = 4 * 10^7$

FIGURE 5: Example of the drag force coefficients provided by the DATCOM software for the configuration $l = 6$ m and $d = 0.8$ m.

(iv) $\beta = [0, 1, 2, 3, 4, 5]$ deg

This means that DATCOM was run 3024 times for each (l, d) combination. The aerodynamic surfaces used in the computation are the cross surfaces of each configuration and correspond to the circular section, that is,

$$S^{(i)} = \pi \left(\frac{d}{2}\right)^2. \quad (13)$$

Figure 5 portrays an example of the aerodynamic coefficients for a single configuration.

4. Rocket Dynamics

The problem investigated in this work consists in finding the sounding rocket with the minimum total volume that can achieve microgravity durations not less than 10 or 15 minutes. In the absence of significant attitude angular velocities, a rocket is considered in microgravity conditions when it is flying at an altitude above 100 km [5].

This approximation is based on real evidence and calculations, allowing for it to be used as a practical rule to analyze the rocket performance. Thus, the problem at hand reduces to finding the minimal rocket volume (l, d) that can guarantee ΔT_{mg} of 10 and 15 min, fixing the propulsive technology (I_{sp}, ϵ) and the geometrical ratios between its parts $(C_{m_0}, C_{ogive}, A_C/A_P, A_T/A_P)$.

4.1. Reference Frames. A description of the reference frames used in this work is useful to understand the guidance implementation. In the following, the notation $R_j(\mp\xi)$ $(j = 1, 2, 3)$ denotes the elementary rotation about axis j by angle ξ while the $\mp$ sign means, respectively, clockwise and counterclockwise.

(1) The *Earth-centered* frame (ECI) $(\hat{\mathbf{c}}_1, \hat{\mathbf{c}}_2, \hat{\mathbf{c}}_3)$ is a Cartesian inertial reference frame defined as follows. Its origin O is the center of the Earth. The unit vector $\hat{\mathbf{c}}_3$ is aligned with the Earth axis of rotation and is positive northward, whereas $\hat{\mathbf{c}}_1$ is aligned with the vernal axis, which corresponds to the intersection of the Earth equatorial plane with the ecliptic plane.

(2) The *Earth-centered Earth-fixed* frame (ECEF) $(\hat{\mathbf{i}}, \hat{\mathbf{j}}, \hat{\mathbf{k}})$ represents a reference system that is rigidly attached to the Earth. Under the assumption that

the planet rotates with a constant angular rate ω_E, also the ECEF frame rotates with angular rate ω_E. The origin of the coordinate system is the center of the Earth, while the unit vector $\hat{\mathbf{i}}$ intersects the Greenwich reference meridian at all times, and $\hat{\mathbf{k}}$ is aligned with the planet axis of rotation and is positive northward. $\omega_E\hat{\mathbf{k}}$ is the vector rotation rate of the ECEF frame with respect to the ECI frame. The reference meridian is the Greenwich side real-time θ_G, given by $\theta_G(t) = \theta_G(\bar{t}) + \omega_E(t - \bar{t})$ where $\bar{t}$ refers to a generic time instant. The ECEF frame is obtained through a counterclockwise rotation by angle θ_G around the third axis, that is, $[\hat{\mathbf{i}}, \hat{\mathbf{j}}, \hat{\mathbf{k}}]^T = R_3(\theta_G)[\hat{\mathbf{c}}_1, \hat{\mathbf{c}}_2, \hat{\mathbf{c}}_3]^T$.

(3) The *local horizontal* frame (LH) $(\hat{\mathbf{r}}, \hat{\mathbf{E}}, \hat{\mathbf{N}})$ is a reference system with the origin in the rocket center of mass. Specifically, $\hat{\mathbf{r}}$ is the unit vector aligned with the instantaneous position $\hat{\mathbf{r}}$, $\hat{\mathbf{E}}$ is directed along the local east direction, and $\hat{\mathbf{N}}$ is aligned with the local north direction. LH frame is obtained from the ECEF frame through the following rotations: $[\hat{\mathbf{r}}, \hat{\mathbf{E}}, \hat{\mathbf{N}}]^T = R_2(-\mathrm{La})R_3(\lambda_g)[\hat{\mathbf{i}}, \hat{\mathbf{j}}, \hat{\mathbf{k}}]^T$.

(4) The *auxiliary orbital* frame (AO) $(\hat{\mathbf{r}}, \hat{\boldsymbol{\theta}}_r, \hat{\mathbf{h}}_r)$ is defined making reference to the rocket relative velocity $v_R = v_I - \omega_E \times r$. The unit vector $\hat{\boldsymbol{\theta}}_R$ is aligned with the projection of the velocity v_r onto the horizontal plane $(\hat{\mathbf{E}}, \hat{\mathbf{N}})$. The AO frame is obtained from the LH frame with the simple rotation $[\hat{\mathbf{r}}, \hat{\boldsymbol{\theta}}_R, \hat{\mathbf{h}}_R]^T = R_1(\zeta_R)[\hat{\mathbf{r}}, \hat{\mathbf{E}}, \hat{\mathbf{N}}]^T$.

(5) The *relative velocity* frame (RV) $(\hat{\mathbf{n}}_R, \hat{\mathbf{v}}_R, \hat{\mathbf{h}}_R)$ is obtained from the AO frame through the following clockwise rotation: $[\hat{\mathbf{n}}_R, \hat{\mathbf{v}}_R, \hat{\mathbf{h}}_R]^T = R_3(-\gamma_R)[\hat{\mathbf{r}}, \hat{\boldsymbol{\theta}}_R, \hat{\mathbf{h}}_R]^T$.

(6) The *wind axis* frame (WA) $(\hat{\mathbf{n}}_W, \hat{\mathbf{v}}_W, \hat{\mathbf{h}}_W)$ is defined with reference to the rocket velocity with respect to the local velocity of the atmosphere $v_a = \omega_E \times r$ so $v_a = v_R$ and just a counterclockwise rotation about axis 2 by the bank angle σ: $[\hat{\mathbf{n}}_W, \hat{\mathbf{v}}_W, \hat{\mathbf{h}}_W]^T = R_2(\sigma)[\hat{\mathbf{n}}_R, \hat{\mathbf{v}}_R, \hat{\mathbf{h}}_R]^T$.

(7) The *auxiliary body axis* frame (ABA) $(\hat{\mathbf{i}}_B, \hat{\mathbf{j}}_B, \hat{\mathbf{k}}_B)$ is a reference system aligned with the rocket inertia axes. The unit vector $\hat{\mathbf{k}}_B$ is orthogonal to the rocket plane of symmetry, while the two remaining unit vectors lie on it. The ABA frame is obtained from the WA frame through a sequence of two rotations: $\sigma[\hat{\mathbf{i}}_B, \hat{\mathbf{j}}_B, \hat{\mathbf{k}}_B]^T = R_3(-\alpha)R_1(\beta)[\hat{\mathbf{n}}_W, \hat{\mathbf{v}}_W, \hat{\mathbf{h}}_W]^T$.

(8) The *body axis* (BA) $(\hat{\mathbf{x}}_B, \hat{\mathbf{y}}_B, \hat{\mathbf{z}}_B)$ is, like the ABA frame, also attached to the rocket inertial axes only with a different orientation. Specifically, $\hat{\mathbf{x}}_B$ is aligned with the rocket longitudinal axis $(\hat{\mathbf{x}}_B = \hat{\mathbf{j}}_B)$; $\hat{\mathbf{z}}_B$ is directed downward so $\hat{\mathbf{z}}_B = -\hat{\mathbf{i}}_B$ and as consequence $\hat{\mathbf{y}}_B = -\hat{\mathbf{k}}_B$. These relations lead to the following elementary rotation:

$$\begin{bmatrix} \hat{\mathbf{x}}_B \\ \hat{\mathbf{y}}_B \\ \hat{\mathbf{z}}_B \end{bmatrix} = \begin{bmatrix} 0 & 1 & 0 \\ 0 & 0 & -1 \\ -1 & 0 & 0 \end{bmatrix} \begin{bmatrix} \hat{\mathbf{i}}_B \\ \hat{\mathbf{j}}_B \\ \hat{\mathbf{k}}_B \end{bmatrix} = R_A \begin{bmatrix} \hat{\mathbf{i}}_B \\ \hat{\mathbf{j}}_B \\ \hat{\mathbf{k}}_B \end{bmatrix}. \tag{14}$$

The knowledge of the instantaneous orientation of $(\hat{\mathbf{x}}_B, \hat{\mathbf{y}}_B, \hat{\mathbf{z}}_B)$ is equivalent to identifying the instantaneous attitude of the rocket.

(9) The *launch inertial* frame (LI) $(\hat{\mathbf{i}}_0, \hat{\mathbf{j}}_0, \hat{\mathbf{k}}_0)$ is an inertial system centered in the launch location at the launch instant. The unit vector $\hat{\mathbf{i}}_0$ is aligned with the local north direction, $\hat{\mathbf{j}}_0$ is directed toward the local east direction, and $\hat{\mathbf{k}}_0$ is aligned with the downward direction. The LI frame is obtained from the ECI frame with a sequence of three rotations: the first two of them take the ECI frame to an intermediary reference frame, named *auxiliary launch inertial* frame (ALI) $(\hat{\mathbf{r}}_0, \hat{\mathbf{E}}_0, \hat{\mathbf{n}}_0)$ using the geographical latitude and longitude of the launch base at the launch time, while the third one relates the axes of the ALI frame to the LI frame. The complete sequence is as follows:

$$\begin{aligned} \begin{bmatrix} \hat{\mathbf{i}}_0 \\ \hat{\mathbf{j}}_0 \\ \hat{\mathbf{k}}_0 \end{bmatrix} &= R_2(-L_L)R_3(\lambda_{aL}) \begin{bmatrix} 0 & 0 & 1 \\ 0 & 1 & 0 \\ -1 & 0 & 0 \end{bmatrix} \begin{bmatrix} \hat{\mathbf{c}}_1 \\ \hat{\mathbf{c}}_2 \\ \hat{\mathbf{c}}_3 \end{bmatrix} \\ &= R_2(-L_L)R_3(\lambda_{aL})R_B \begin{bmatrix} \hat{\mathbf{c}}_1 \\ \hat{\mathbf{c}}_2 \\ \hat{\mathbf{c}}_3 \end{bmatrix}. \end{aligned} \tag{15}$$

The BA frame is also related to the LI frame through a sequence of three rotations using the attitude angles (ϕ, θ, ψ). The complete sequence is $[\hat{\mathbf{x}}_B, \hat{\mathbf{y}}_B, \hat{\mathbf{z}}_B]^T = R_1(\phi)R_2(\theta)R_3(\psi)[\hat{\mathbf{i}}_0, \hat{\mathbf{j}}_0, \hat{\mathbf{k}}_0]^T$.

In order to avoid ambiguities in the definition of the vectors of interest, the angles introduced in this section have to be constrained. Table 3 shows the limitation for the angles used in this work.

Any vector can be obtained with respect to any reference frame using the rotations defined in this section. These rotations can be used to define the rocket kinematics and dynamics through the motion, and Figures 6 and 7 portray all the reference frames used in this work, together with the related rotations.

Table 3: Angle constraints.

$-\pi < \theta_G \le \pi$	$-\pi < \lambda_G \le \pi$
$-\frac{\pi}{2} < \mathrm{La} \le \frac{\pi}{2}$	$-\pi < \zeta_R \le \pi$
$-\frac{\pi}{2} < \gamma_R \le \frac{\pi}{2}$	$-\pi < \sigma \le \pi$
$-\frac{\pi}{2} < \beta \le \frac{\pi}{2}$	$-\pi < \alpha \le \pi$
$-\pi < \psi \le \pi$	$-\frac{\pi}{2} < \theta \le \frac{\pi}{2}$
$-\pi < \phi \le \pi$	—

4.2. Forces. The main term of the gravitational force G is given in the RV frame simply by

$$\frac{G}{m} = -\frac{\mu_E}{r^3} = -\frac{\mu_E}{r^2}\begin{bmatrix}\cos\gamma_R\\ \sin\gamma_R\\ 0\end{bmatrix}^T\begin{bmatrix}\hat{\mathbf{n}}_R\\ \hat{\mathbf{v}}_R\\ \hat{\mathbf{h}}_R\end{bmatrix}. \tag{16}$$

The components of the aerodynamic force can be referred to the WA frame and then projected in the RV frame with a simple rotation. The three components are the lift force, the drag force, and the side force.

$$\frac{A}{m} = \frac{L+D+Q}{m} = \frac{L\hat{\mathbf{n}}_W - D\hat{\mathbf{v}}_W + Q\hat{\mathbf{h}}_W}{m}, \tag{17}$$

where

$$\begin{aligned}
L &= L\hat{\mathbf{n}}_W = \frac{1}{2}\rho v_W^2 C_L(\alpha,\beta,\mathrm{Re},M)\hat{\mathbf{n}}_W,\\
D &= -D\hat{\mathbf{n}}_W = -\frac{1}{2}\rho v_W^2 C_D(\alpha,\beta,\mathrm{Re},M)\hat{\mathbf{n}}_W,\\
Q &= Q\hat{\mathbf{n}}_W = \frac{1}{2}\rho v_W^2 C_Q(\alpha,\beta,\mathrm{Re},M)\hat{\mathbf{n}}_W.
\end{aligned} \tag{18}$$

The aerodynamic forces have to be projected in the RV frame with a rotation about the bank angle around the second axis:

$$A = [A_n A_v A_h]\begin{bmatrix}\hat{\mathbf{n}}_R\\ \hat{\mathbf{v}}_R\\ \hat{\mathbf{h}}_R\end{bmatrix} = [L - DQ]R_2(\sigma)\begin{bmatrix}\hat{\mathbf{n}}_R\\ \hat{\mathbf{v}}_R\\ \hat{\mathbf{h}}_R\end{bmatrix}. \tag{19}$$

The aerodynamic forces are taken into account up to 100 km of altitude where the atmospheric density becomes negligible.

The thrust can be projected along the RV frame with the in-plane α_T and the out-of-plane β_T:

$$\begin{aligned}
\frac{\mathbf{T}}{m} &= \begin{bmatrix}\frac{\mathbf{T}}{m}\cos\beta_T\sin\alpha_T & \frac{\mathbf{T}}{m}\cos\beta_T\cos\alpha_T & \frac{\mathbf{T}}{m}\sin\beta_T\end{bmatrix}\\
&\quad\cdot\begin{bmatrix}\hat{\mathbf{n}}_R & \hat{\mathbf{v}}_R & \hat{\mathbf{h}}_R\end{bmatrix}^T,
\end{aligned} \tag{20}$$

and to avoid ambiguities, the following constraints must hold:

$$\begin{gathered}
-\pi < \alpha_T \le \pi,\\
-\frac{\pi}{2} \le \beta_T \le \frac{\pi}{2}.
\end{gathered} \tag{21}$$

The thrust vector $\mathbf{T}$ is considered aligned with the rocket longitudinal axis so two angles, α_T and β_T suffices to describe its direction.

4.3. Equations of Motion. The equations of motion that govern the three-dimensional rocket dynamics can be conveniently written in terms of $\{r,\lambda_G,\mathrm{La},\gamma_R,v_R,\zeta_R\}$. These variables refer to the relative motion in the RV frame. They form the state vector $\mathbf{x}_R$ of the launch vehicle (in rotating coordinates).

$$\begin{aligned}
\dot{r} &= v_R\sin\gamma_R,\\
\dot{\lambda}_G &= \frac{v_R\cos\gamma_R\cos\zeta_R}{r\cos\mathrm{La}},\\
\dot{\mathrm{La}} &= \frac{v_R\cos\gamma_R\sin\zeta_R}{r},\\
\dot{\gamma}_R &= \left(-\frac{\mu_E}{v_R r^2} + \frac{v_R}{r}\right)\cos\gamma_R + \frac{(T/m)\cos\beta_T\sin\alpha_T}{v_R} + \frac{A_n}{v_R}\\
&\quad + \frac{\omega_E^2 r}{v_R}(\cos\mathrm{La}(\cos\mathrm{La}\cos\gamma_R + \sin\mathrm{La}\sin\gamma_R\sin\zeta_R))\\
&\quad + 2\omega_E\cos\mathrm{La}\cos\zeta_R,\\
\dot{v}_R &= -\frac{\mu_E}{r^2}\sin\gamma_R + \frac{T}{m}\cos\beta_T\cos\alpha_T + A_v\\
&\quad + \omega_E^2 r\cos\mathrm{La}(\cos\mathrm{La}\sin\gamma_R - \sin\mathrm{La}\cos\gamma_R\sin\zeta_R),\\
\dot{\zeta}_R &= -\frac{v_R}{r}\tan\mathrm{La}\cos\gamma_R\cos\zeta_R + \frac{T/m}{v_R\cos\gamma_R}\sin\beta_T\\
&\quad + 2\omega_E\cos\mathrm{La}\tan\gamma_R\sin\zeta_R + \frac{A_h}{v_R\cos\gamma_R}\\
&\quad - \frac{\omega_E^2 r}{v_R\cos\gamma_R}\sin\mathrm{La}\cos\mathrm{La}\cos\zeta_R - 2\omega_E\sin\mathrm{La}.
\end{aligned} \tag{22}$$

The initial values for (22) are reported in Table 4.

Equation (22) is valid for both the propelled arc and the ballistic flight of the ogive. The values for La and λ_G in Table 4 are referred to the Malindi launch base, while the launch is in the east direction (ζ_R). The control laws for (α_T,β_T), are determined using three distinct guidance scheme, namely, the constant attitude guidance, the near radial guidance, and the sun-pointing guidance, which are described in the following section. The state $\mathbf{x}_R$ is continuos across the first stage separation, which occurs at time t_B. After that, the payload continues its motion in a ballistic trajectory.

5. Guidance Algorithms

5.1. Constant Attitude Guidance. With this guidance, the rocket orientation does not change during the flight and

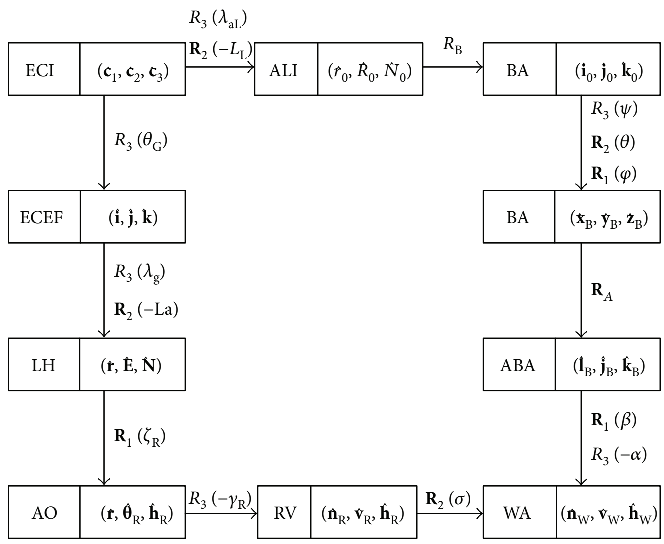

Figure 6: Reference frames and related rotation matrices.

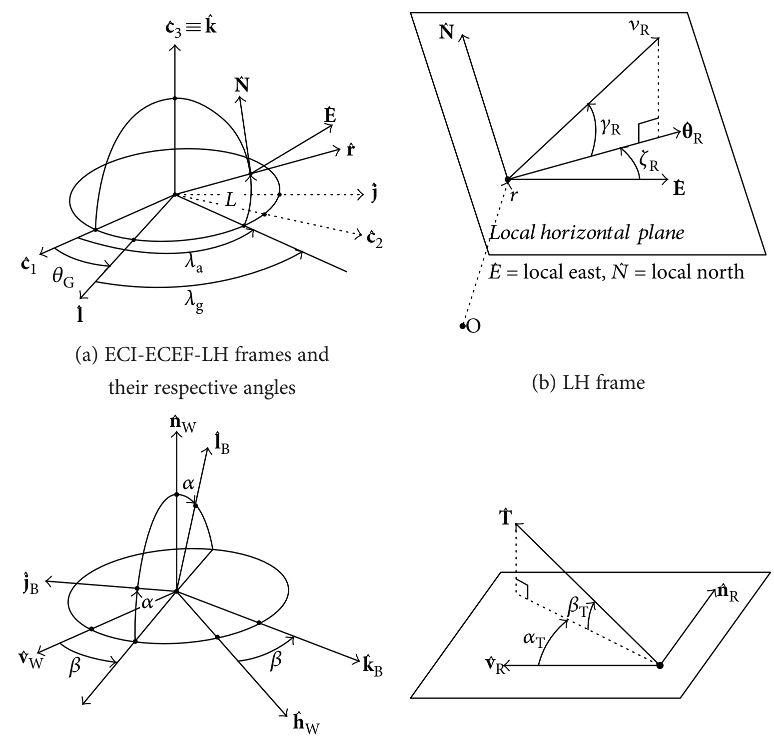

(a) ECI-ECEF-LH frames and their respective angles

(b) LH frame

(c) WA-ABA frames and their relative angles

(d) Thrust vector direction with respect to the RV frame

Figure 7: Main reference frames and related angles.

was actually implemented in the Black Brant X (cf. [17]). This is ideal to achieve nominal (perfect) microgravity conditions ($\Delta g = 0$), due to rotation rates equal to 0. The attitude angles $\{\phi, \theta, \psi\}$ remain constant; therefore, in this type of guidance, the following expressions can be assumed as follows:

$$\phi = \phi_0 \theta = \theta_0 \psi = \psi_0. \quad (23)$$

Table 4: Initial condition for (22).

r (km)	R_E+0.001
v_R (km/s)	0.008
γ_R (deg)	86
La (deg)	−2.938
ζ_R (deg)	0
λ_G (deg)	40.213

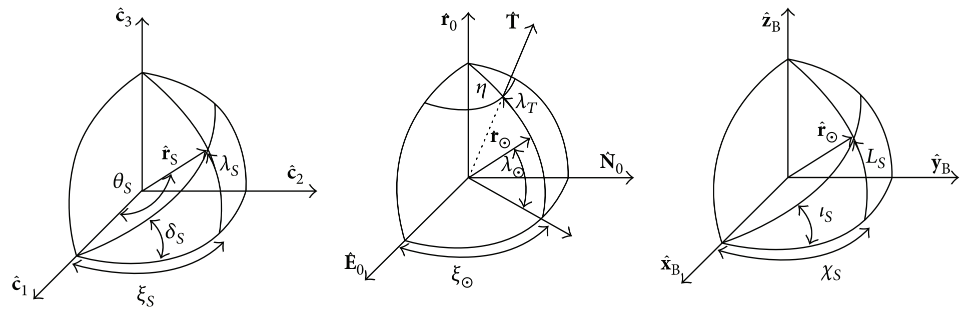

(a) Sun position $\hat{\mathbf{r}}_S$ in the ECI frame

(b) Sun position $\hat{\mathbf{r}}_\odot$ in the ALI frame. This case is an example of the sun being outside the spherical section allowed by η

(c) Sun position $\hat{\mathbf{r}}_\odot$ in the BA frame. χ_S and L_S are obtained projecting ι_S on the BA frame

Figure 8: Sun-pointing guidance principal angles and axes.

The remaining angles $\{\alpha_T, \beta_T, \alpha, \beta, \sigma\}$ can be found using analytical formulas at any times using the rotation matrices portrayed in Figure 6.

5.2. Near Radial Guidance. This guidance is called near radial because it is defined in the AO reference frame and the thrust direction is defined by

$$\alpha_T = \gamma_{R0} + \frac{t}{t_B}\left(\frac{\pi}{2} - \gamma_{R0}\right) - \gamma_R, \qquad \beta_T = 0 \tag{24}$$

whereas $\gamma_{R0} = \theta_0$ is the pitch angle at the initial time and is equal to the initial flight path angle. With $\beta_T = 0$, the angle that the rocket forms with the local horizontal axis is given by $(\alpha_T + \gamma_R)$. At the initial time, this angle corresponds to the initial flight path angle, while at the burnout time, it corresponds to $(\alpha_T + \gamma_R) = \pi/2$. The roll angle is can be chosen arbitrarily and is set to 0 deg. For the remaining angles $\{\theta, \psi, \alpha, \beta, \sigma\}$, they are obtained through analytical expressions through the rotation matrices in Figure 6. The thrust direction tends to be aligned with the radial direction. Thus, in principle, this guidance leads to obtain the mean maximal altitude for the rocket at hand. Moreover, with this guidance, the usual values of Δg are in the order of 10^{-4}m/sec^2.

5.3. Sun-Pointing Guidance. The sun-pointing guidance is based on maintaining constant attitude of the rocket with respect to the sun position. The attitude angles $\{\phi, \theta, \psi\}$ are computed in an analytical fashion using the rotations in Figure 6. The first step to obtain the attitude of the sounding rocket is to locate the sun position with respect to the ECI frame:

$$\hat{r}_S = [\cos\lambda_S \cos\xi_S \quad \cos\lambda_S \sin\xi_S \quad \sin\lambda_S][\hat{\mathbf{c}}_1 \quad \hat{\mathbf{c}}_2 \quad \hat{\mathbf{c}}_3]^T, \tag{25}$$

where λ_S and ξ_S are the sun declination and the right ascension, respectively. Then, projection of this unit vector into the ALI frame yields as follows:

$$\begin{aligned}\hat{\mathbf{r}}_\odot &= \hat{\mathbf{r}}_S R_3(-\lambda_{aL}) R_2(L_L) \begin{bmatrix} \hat{\mathbf{r}}_0 \\ \hat{\mathbf{E}}_0 \\ \hat{\mathbf{N}}_0 \end{bmatrix} \\ &= [\cos\lambda_\odot \cos\xi_\odot \quad \cos\lambda_\odot \sin\xi_\odot \quad \sin\lambda_\odot] \begin{bmatrix} \hat{\mathbf{r}}_0 \\ \hat{\mathbf{E}}_0 \\ \hat{\mathbf{N}}_0 \end{bmatrix} \\ &= [X_\odot \quad Y_\odot \quad Z_\odot] \begin{bmatrix} \hat{\mathbf{r}}_0 \\ \hat{\mathbf{E}}_0 \\ \hat{\mathbf{N}}_0 \end{bmatrix}.\end{aligned} \tag{26}$$

So the thrust direction is obtained by aligning the body axis of the launcher with the sun direction in the ALI frame, as shown in Figure 8. To avoid that the rocket will fly with a γ_r near to zero while trying to catch the sun slightly above the local horizon, the thrust direction is constrained to have a displacement from $\hat{\mathbf{r}}_\odot$ not exceeding the maximal value $\eta = 10$deg (cf. Figure 8). So the thrust direction is defined imposing $\xi_T = \xi_\odot$ and $\lambda_T = \max(\lambda_\odot, \pi/2 - \eta)$. The angles α_T and β_T are then obtained through rotation of $\hat{\mathbf{T}}$ from the ALI frame to the RV frame using the rotations reported in Figure 6 and considering that the thrust is aligned with the longitudinal axis of the rocket $\hat{\mathbf{x}}_B$. The pitch and yaw angles are then obtained with the following expressions:

$$\begin{aligned}\sin\theta &= \cos\lambda_T \cos\xi_T \longrightarrow \theta, \\ \cos\psi &= \sin\lambda_T, \\ \sin\psi &= \cos\lambda_T \sin\xi_T \longrightarrow \psi.\end{aligned} \tag{27}$$

As roll angle is arbitrary, it can be selected after choosing the angle ι_S related to the sun position in the body frame. The roll angle ϕ is obtained by comparing $\hat{\mathbf{r}}_\odot$ in the ALI frame with its projection in the RV frame.

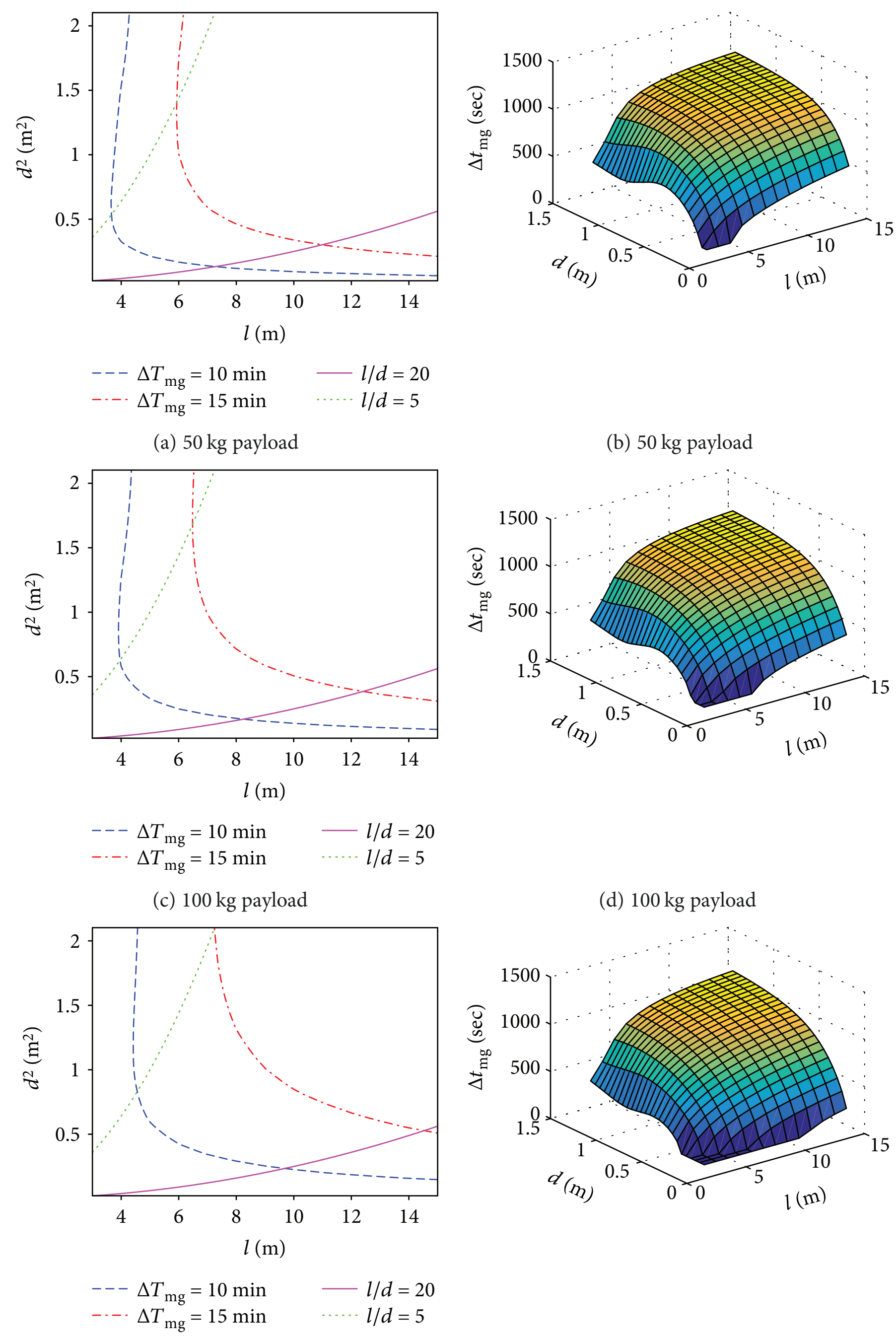

(a) 50 kg payload

(b) 50 kg payload

(c) 100 kg payload

(d) 100 kg payload

(e) 200 kg payload

(f) 200 kg payload

Figure 9: Optimal results for the constant attitude guidance.

From Figure 8(c), it is straightforward to obtain the following angles:

$$\frac{\sin L_S}{\sin \iota_S} = \sin \lambda_T \to L_S,$$
$$\frac{\tan L_S}{\tan \iota_S} = \sin \xi_S, \tag{28}$$
$$\frac{\cos \lambda_T}{\cos L_S} = \cos \xi_S \to \xi_S.$$

They univocally define the vector $\hat{\mathbf{r}}_\odot = [X_{B\odot} Y_{B\odot} Z_{B\odot}, \hat{\mathbf{x}}_B \hat{\mathbf{y}}_B \hat{\mathbf{z}}_B]^T$ in the body frame. Comparing the coordinates of $\hat{\mathbf{r}}_\odot$ in the ALI frame to the ones in the BA frame leads the following expression:

$$\begin{aligned}[X_\odot \quad Y_\odot \quad Z_\odot] R_B{}^T R_3{}^T(\psi) R_2{}^T(\theta) R_1{}^T(\phi) \\ = [X_{B\odot} \quad Y_{B\odot} \quad Z_{B\odot}].\end{aligned} \tag{29}$$

Equation (29) leads to the roll angle ϕ.

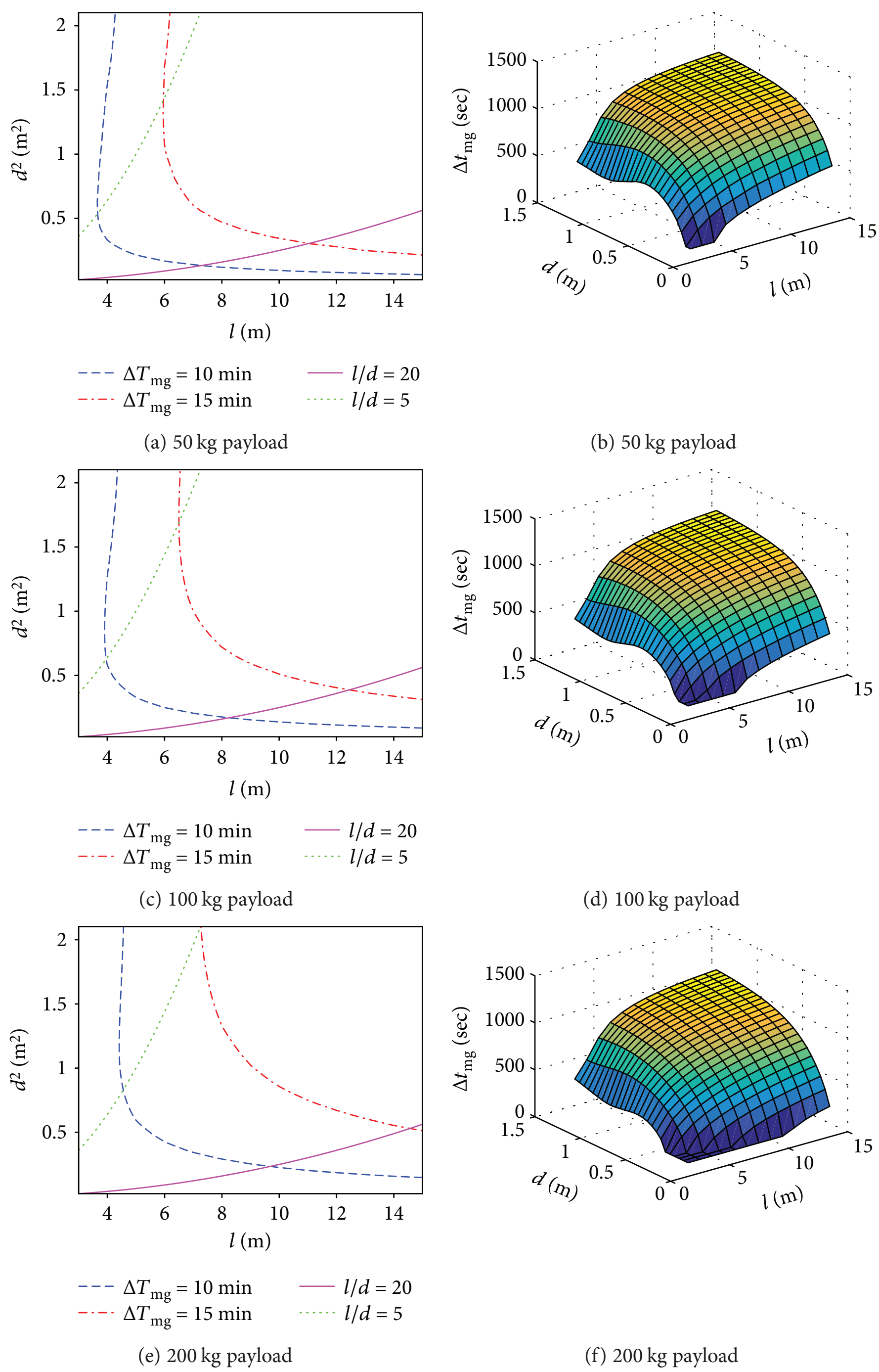

(a) 50 kg payload
(b) 50 kg payload
(c) 100 kg payload
(d) 100 kg payload
(e) 200 kg payload
(f) 200 kg payload

Figure 10: Optimal results for the near radial guidance.

Then, the aerodynamic angles α, β, σ can be obtained through the rotation matrices in Figure 6, which are not reported for the sake of brevity. In short, the sun-pointing guidance requires specifying the following parameters:

(i) θ_S which is the sun position in the ECI frame

(ii) η which constraints the possible thrust direction

(iii) θ_{G0}, defined by the date and hour of the launch

(iv) ι_S, needed to obtain the roll angle ϕ

As the attitude is also in this case constant, the sun-pointing guidance is a particular case of the constant attitude guidance. Hence, it maintains its main advantages like the ideally perfect microgravity condition ($\Delta g = 0$) and can provide the perfect conditions for thermal experiments in the space.

6. Numerical Results

Figures 9–11 portray the results of the computation, which are, respectively, for the constant attitude guidance

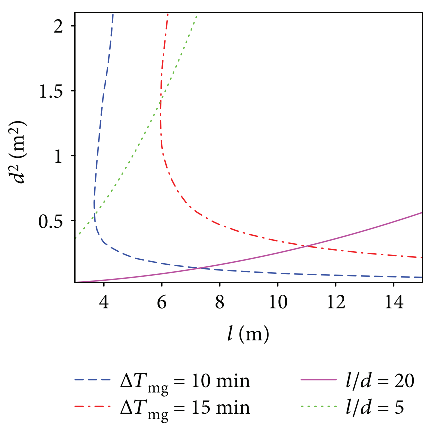

(a) 50 kg payload

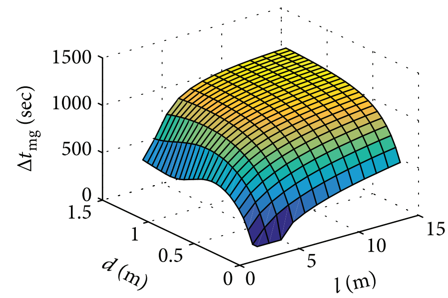

(b) 50 kg payload

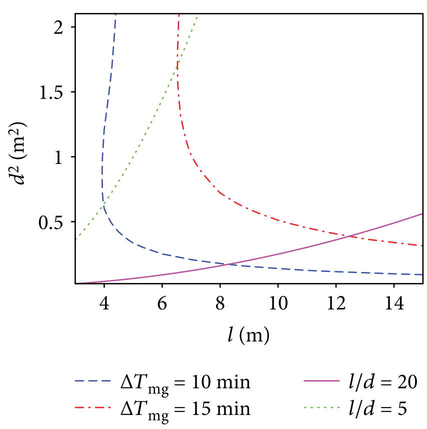

(c) 100 kg payload

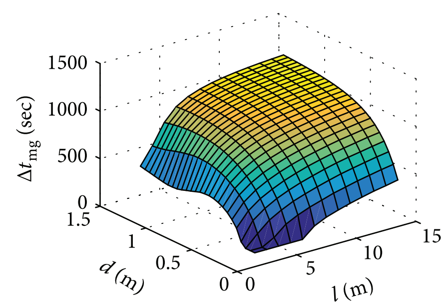

(d) 100 kg payload

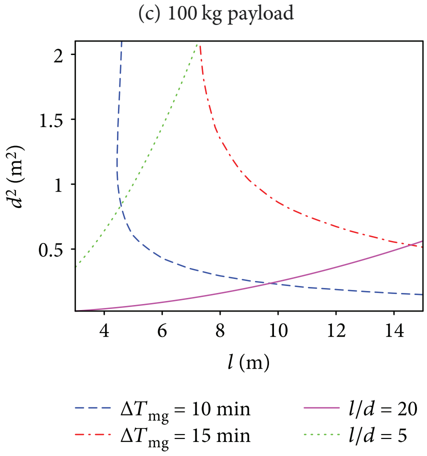

(e) 200 kg payload

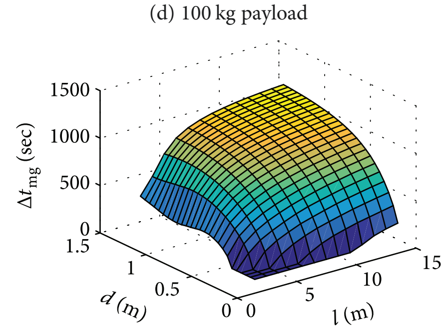

(f) 200 kg payload

Figure 11: Optimal results for the sun-pointing guidance.

Table 5: Optimal configurations for each payload mass, ΔT_{mg} = 10 min.

m_U (kg)	50	100	200
l (m)	7.29	8.25	9.69
d (m)	0.36	0.41	0.48

Table 6: Optimal configurations for each payload mass, ΔT_{mg} = 15 min.

m_U (kg)	50	100	200
l (m)	10.98	12.42	14.53
d (m)	0.55	0.62	0.73

(Figure 9), the near radial guidance (Figure 10), and the sun-pointing guidance (Figure 11). From Figure 9 to Figures 11(b), 11(d), and 11(f)), if the desired ΔT_{mg} is not chosen, it is possible to obtain a maximum ΔT_{mg} for each length. This result is particularly visible for the shorter lengths while is less evident for the bigger configurations.

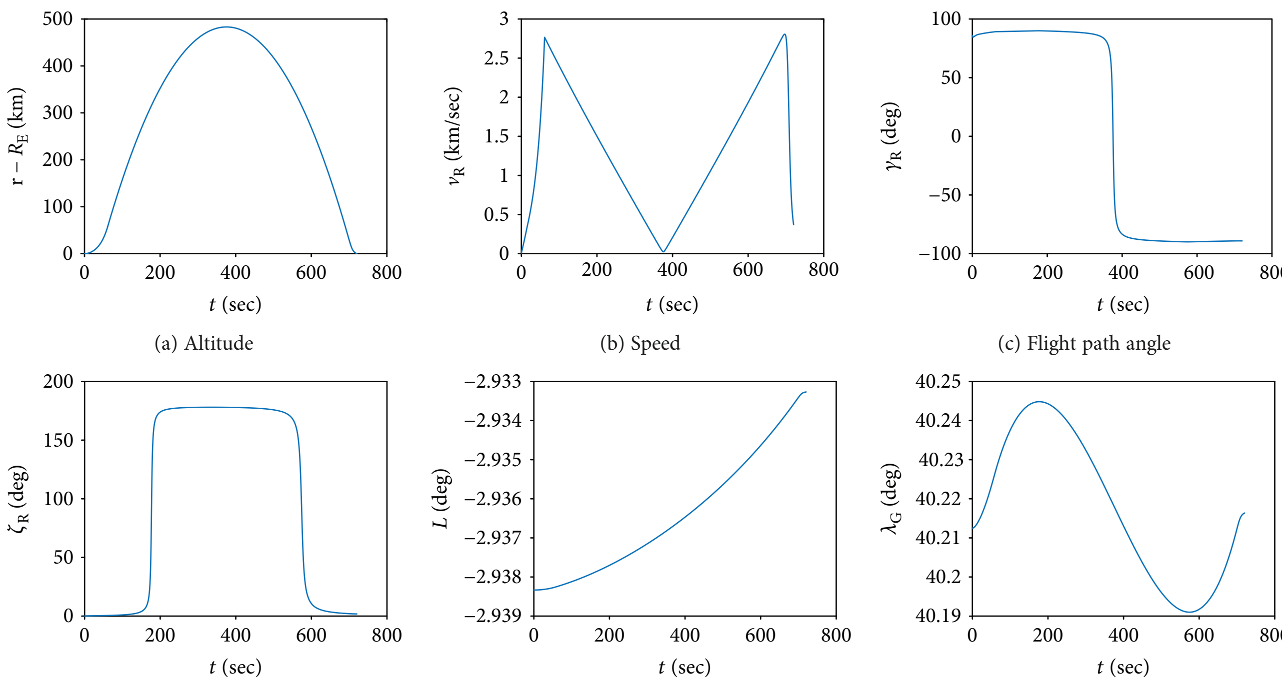

(a) Altitude (b) Speed (c) Flight path angle

(d) Heading angle (e) Latitude (f) Longitude

FIGURE 12: State variables for the configuration with $l = 7.29$ m and $d = 0.36$ m (near radial guidance).

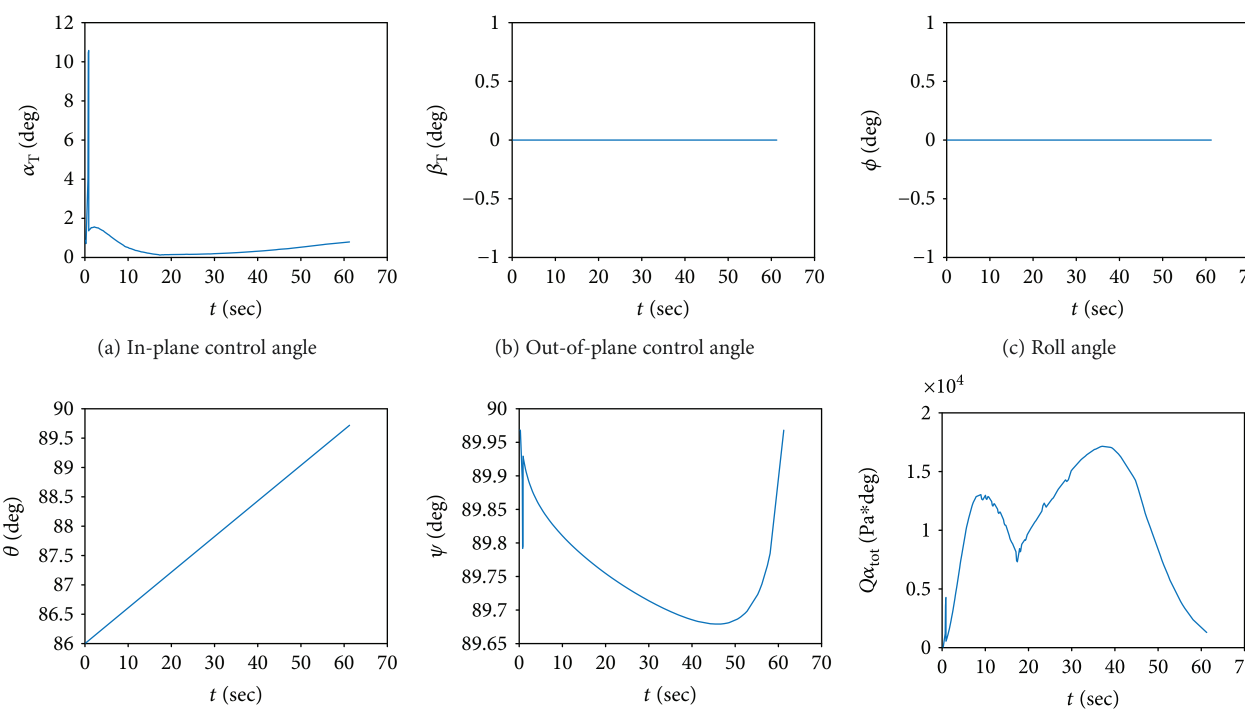

(a) In-plane control angle (b) Out-of-plane control angle (c) Roll angle

(d) Pitch angle (e) Yaw angle (f) Dynamic pressure constraint

FIGURE 13: Control law, attitude angles, and dynamic pressure in the thrust arc for the configuration with $l = 7.29$ m and $d = 0.36$ m (near radial guidance).

Panels (a), (c), and (e) of Figures 9–11 show every (l, d) combination which guarantee 600 and 900 sec of ΔT_{mg}. The optimal configuration corresponds to the point in which each curve is tangent to an equilateral isovolume hyperbola in the (l, d^2) graph. As the tangence point always occurs in the lowest right part of the graph, two constraints were

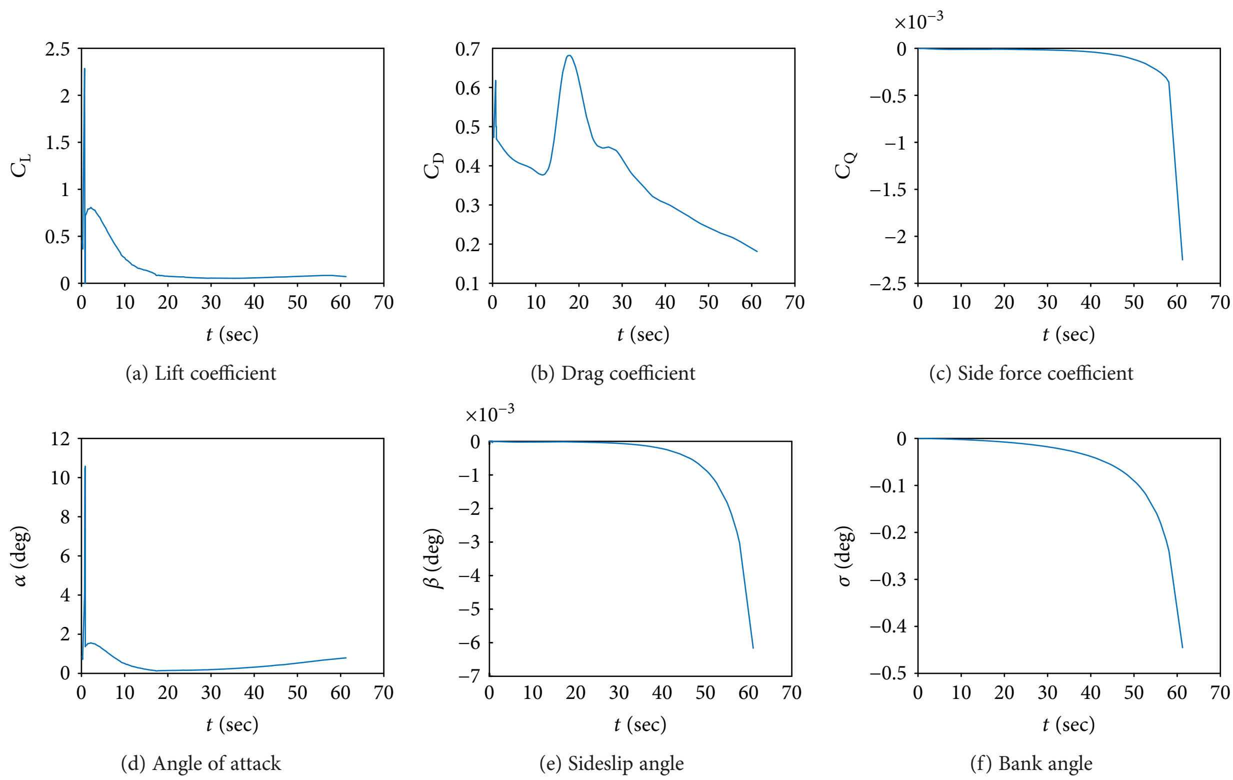

(a) Lift coefficient (b) Drag coefficient (c) Side force coefficient

(d) Angle of attack (e) Sideslip angle (f) Bank angle

FIGURE 14: Aerodynamic angles and coefficients in the thrust arc for the configuration with $l = 7.29$ m and $d = 0.36$ m (near radial guidance).

inserted, for the sake of avoiding too slender or bulky configurations. In general, the constraint for the l/d is

$$5 \le \frac{l}{d} \le 20. \quad (30)$$

It should be noticed that that the optimal configurations for all the three guidance are nearly the same, and this means that the preliminary design of the sounding rocket can be done regardless of the guidance type. Tables 5 and 6 show the optimal rocket configuration for 600 and 900 sec of ΔT_{mg} and for all the payload masses. The configuration with $l = 7.29$m and $d = 0.36$m in Table 5 is particularly similar to the Black Brant VC, demonstrating that with similar m_U and ΔT_{mg}, the algorithm can be effective to optimize the size of the rocket.

Figures 12–14 portray the complete state vector elements and other variables for the optimal configuration with $m_U = 50$ kg and $\Delta T_{\text{mg}} = 10$ min, using the near radial guidance.

For the rocket structural integrity, the constraint $Q\alpha_{\text{tot}} < 150000\text{Pa} * \text{deg}$ must be satisfied, where

$$Q = \frac{1}{2}\rho v_R^2 \quad (31)$$

and

$$\alpha_{\text{tot}} = \arccos(\cos\alpha \cos\beta). \quad (32)$$

From Figure 13(f), it is apparent that the constraint is satisfied, and the same occurs for all the cases.

7. Conclusions

Designing a sounding rocket is a difficult task, and this work proposes a method to simplify the early stage modeling process and performance evaluation. The new methodology at hand has four principal phases: (i) mass and geometry sizing based on reasonable assumptions, (ii) scaled propulsion modeling, (iii) accurate aerodynamic modeling, and (iv) the performance evaluation using different guidance schemes. With regard to the guidance algorithms, three schemes where presented which are the constant attitude, near radial, and sun-pointing guidances. While the constant attitude guidance is a well-known scheme, the other two are novel guidances. In particular, the benefits of the sun-pointing guidance are presented, which are the nearly perfect microgravity condition and the possibility to orient the rocket with a defined attitude with respect to the sun. The results clearly show that the algorithm is capable of providing a fast and reasonable sizing in accordance with the mission requirements. The results obtained can be used as a reference point for a montecarlo campaign to analyze the impact points in the presence of local winds or as a first guess solution for more sophisticated optimization algorithms.

Nomenclature

g: Earth gravitational acceleration, m/sec^2
μ_E: Earth gravitational parameter, km^2/sec^3
d: Rocket diameter, m
l_{ogive}: Ogive length, m
C_{m_0}: Dimensionless total initial mass

m_0: Initial mass, kg
m_P: Propellant mass, kg
V_{body}: Rocket volume, m^3
u: Mass ratio
T: Thrust, N
I_{SP}: Specific impulse, sec
t_B: Burnout time, sec
C_L: Lift coefficient
C_Q: Side force coefficient
D: Drag force, N
M: Mach number
α: Angle of attack, deg
S: Reference surface, m^2
ΔT_{mg}: Microgravity duration, sec
θ_G: Greenwich sidereal time, deg
L_L: Launch base latitude, deg
λ_G: Longitude, deg
v_R: Relative velocity m/sec^2
σ: Bank angle, deg
θ: Pitch angle, deg
α_T: In-plane control angle, deg
m: Mass, kg
$\lambda_{\odot}$: Sun declination ALI frame, deg
λ_S: Sun declination ECI frame, deg
λ_T: Thrust declination ALI frame, deg
L_S: Sun declination BA frame, deg
ω_E: Earth rotation rate, deg/sec^2
l: Rocket total length, m
t: Time, sec
l_{body}: Rocket body length, m
C_{ogive}: Dimensionless ogive length
m_{aux}: Auxiliary mass, kg
m_S: Structural mass, kg
ϵ: Structural coefficient
m_U: Payload mass, kg
n_0: Acceleration at launch, g
$\dot{m}$: Mass rate, kg/sec
m_{0body}: Cylinder initial mass, kg
C_D: Drag coefficient
L: Lift force, N
Q: Side force, N
Re: Reynolds number
β: Sideslip angle, deg
ρ: Atmospheric density, kg/m^3
r: Radius, m
La: Latitude, deg
λ_{aL}: Launch base longitude, deg
γ_R: Relative flight path angle, deg
ζ_R: Heading angle, deg
ϕ: Roll angle, deg
ψ: Yaw angle, deg
β_T: Out-of-plane control angle, deg
Q: Dynamic pressure, Pa
$\xi_{\odot}$: Sun right ascension ALI frame, deg
ξ_S: Sun right ascension ECI frame, deg
ξ_T: Thrust right ascension ALI frame, deg
χ_S: Sun right ascension BA frame, deg.

Conflicts of Interest

The authors declare that they have no conflicts of interest.

References

[1] A. Asensio Ramos and R. Manso Sainz, "Signal detection for spectroscopy and polarimetry," *Astronomy and Astrophysics*, vol. 547, p. A113, 2012.

[2] E. Luvsandamdin, S. Spießberger, M. Schiemangk et al., "Development of narrow linewidth, micro-integrated extended cavity diode lasers for quantum optics experiments in space," *Applied Physics B*, vol. 111, no. 2, pp. 255–260, 2013.

[3] S. Wieman, L. Didkovsky, T. Woods, A. Jones, and C. Moore, "Sounding rocket observations of active region soft X-ray spectra between 0.5 and 2.5 nm using a modified SDO/EVE instrument," *Solar Physics*, vol. 291, no. 12, pp. 3567–3582, 2016.

[4] Sounding Rocket Program Handbook, *National Aeronautics and Space Administration, Goddard Space Flight Center*, 2001.

[5] G. Seibert, *The History of Sounding Rockets and Their Controibution to European Space Research*, ESA Publications Division, 2006.

[6] S. M. Chowdhury, J. P. de la Beaujardiere, M. Brooks, and L. Roberts, "An integrated six degree-of-freedom trajectory simulator for hybrid sounding rockets," in *49th AIAA Aerospace Sciences Meeting including the New Horizons Forum and Aerospace Exposition*, Orlando, Florida, January 2011.

[7] S. M. Chowdhury, *Design and Performance Simulation of a Hybrid Sounding Rocket*, Master's thesis, University of Kwa-Zulu-Natal, 2012.

[8] L. Casalino and D. Pastrone, "Optimization of hybrid sounding rockets for hypersonic testing," in *45th AIAA/ASME/SAE/ASEE Joint Propulsion Conference & Exhibit*, Denver, Colorado, August 2009.

[9] L. Casalino and D. Pastrone, "Optimization of hybrid sounding rockets for hypersonic testing," *Journal of Propulsion and Power*, vol. 28, no. 2, pp. 405–411, 2012.

[10] S. Nonaka, H. Ogawa, Y. Naruo, and Y. Inatani, "System design and tecnical demonstrations for reusable sounding rocket," in *20th ESA Symposium on European Rocket and Balloon Programmes and Related Research*, Hyére, France, October 2011.

[11] D. L. Y. Woo and J. A. Martin, "Reusable sounding-rocket design," *Journal of Spacecraft and Rockets*, vol. 32, no. 2, pp. 376–378, 1995.

[12] F. Cremaschi, S. Weikert, A. Wiegand, W. Jung, and F. Scheuerpflug, "Sounding rocket trajectory simulation and optimization with astos," in *19th ESA Symposium on European Rocket and Balloon Programmes and Related Research*, 2009.

[13] W. B. Blake, *Missile DATCOM User's Manual – 1997 Fortran 90 Revision*, United States Air Force, 1998.

[14] L. Mangiacasale, *Meccanica del volo atmosferico. Terne di riferimento, equazioni di moto, linearizzazione, stabilità*, Ingegneria, 2000.

[15] M. Pallone, M. Pontani, and P. Teofilatto, "Accurate modeling and near optimal ascent trajectory of microsatellite launch vehicles via firework algorithm," in *67th International Astronautical Congress*, 2016.

[16] M. Pontani, "Particle swarm optimization of ascent trajectories of multistage launch vehicles," *Acta Astronautica*, vol. 94, no. 2, pp. 852–864, 2014.

[17] L. Ljunge and L. Hall, "S19 guidance of the Black Brant X sounding rocket," *Journal of Guidance, Control, and Dynamics*, vol. 7, no. 2, pp. 156–160, 1984.